# Simulation of dust particles in dual-frequency capacitively coupled silane discharges

Xiang-Mei Liu, Yuan-Hong Song, Xiang Xu, and You-Nian Wang*
*School of Physics and Optoelectronic Technology, Dalian University of Technology, Dalian 116024, People's Republic of China*
(Received 21 September 2009; published 22 January 2010)

The behavior of nanoparticles in dual-frequency capacitively coupled silane discharges is investigated by employing a one-dimensional self-consistent fluid model. The numerical simulation tries to trace the formation, charging, growth, and transport of dust particles during the discharge, under the influences of the high- and low-frequency electric sources, as well as the gas pressure. The effects of the presence of the nanoparticles and larger anions on the plasma properties are also discussed, especially, for the bulk potential, electron temperature, and densities of various particles. The calculation results show that the nanoparticle density and charge distribution are mainly influenced by the voltage and frequency of the high-frequency source, while the voltage of the low-frequency source can also exert an effect on the nanoparticle formation, compared with the frequency. As the discharge lasts, the electric potential and electron density keep decreasing, while the electron temperature gets increasing after a sudden drop.

DOI: 10.1103/PhysRevE.81.016405 PACS number(s): 52.27.Lw, 52.65.−y, 52.80.Pi

## I. INTRODUCTION

Plasma processings have been widely applied for thin-film deposition, etching, and other surface modification in microelectronics and nanotechnology. In such processings, formation of dust particles or nanoparticles in reactive gas plasmas, which cannot be neglected or even can play an important role, has attracted much attention [1]. In the microelectronics manufacturing technique, for example, the formation of dust particles is an unwanted process and usually kept from happening, for they may fall on the substrate the moment plasma discharge quenches and cause unqualified products. On the other hand, dust particles are considered to be helpful to film deposition. It has been found in experimental and theoretical studies that the presence of dust particles can effectively enhance deposition rate in the plasma enhanced chemical vapor deposition (PECVD) processing [2]. Thus, investigations of the formation, charging, growth, and transport of dust particles are very necessary in various plasma discharges.

In PECVD process, thin films of hydrogenated amorphous silicon are deposited and mainly applied in solar cell technology and for the manufacturing of flat panel displays. In recent years, much work has been devoted to silane/hydrogen discharges and particle formation mechanism for radio-frequency capacitively coupled plasmas (CCPs). A one-dimensional fluid model was originally developed by Nienhuis *et al.* [3] to investigate the relation between the external settings and the resulting composition of the gas and the deposition rate, in which the electric field, densities, and fluxes of the particles can be calculated self-consistently. Shortly afterward, Leroy *et al.* [4] developed a two-dimensional fluid model to formulate $SiH_4$-$H_2$ radio-frequency glow discharges in a cylindrical PECVD reactor, in which the experimental values were introduced as input parameters to speed up the calculation. To investigate the important nanoparticle formation mechanism, Gallagher [5,6] put forward a simple homogeneous plasma-chemistry model, mainly, analyzing the measurements of $Si_xH_m^-$ anions and electrons in silane discharges, by adopting the realistic estimates of particle density and mutual neutralization rate coefficients. Enlightened by the experimental results [7] that the nucleation of dust particles happens after a successive chemical reactions, de Bleecker *et al.* [8] analyzed the important precursors of the dust formation and discussed the role of the vibrational excited silane molecules on the formation process in low-pressure silane discharges. Then, a detailed chemical kinetic scheme, including various gas-phase reactions, which would lead to larger clusters, was present in Ref. [9], based on which formation of nanoparticles with a given radius was discussed. Thus, we can obtain a relative entire understanding of the formation, growth, transport, and charging mechanisms of the smaller nanoparticles [10] in the silane discharge.

In plasma processings, a conventional capacitively coupled reactor, driven by only one frequency is extensively used. In this device, however, the ion flux and energy cannot be controlled independently. In the early 1990s, in order to improve the performance of the traditional CCP reactor, a dual-frequency capacitively coupled plasma (DF-CCP) was introduced. In this device, one high-frequency (HF) and one low-frequency (LF) sources are applied to one electrode or two different electrodes [11–14]. The HF source mainly determines the plasma density or ion flux, while the LF source is in charge of the ion bombardment energy. Thus, independent control of high-density plasma and ion energy can be provided. Dual-frequency discharges recently found broad application in the technological processes of depositing $Si_3N_4$ [15] and fluorinated silicon dioxide films [16]. However, so far little research has been devoted to the physics in this aspect. Especially, a comprehensive understanding of the behaviors of nanoparticles under the influence of the dual frequency still remains elusive and, of course, is expected.

In this work, the effects of dual-frequency sources on plasma density, electron temperature, nanoparticle density, and nanoparticle charge in capacitively coupled silane discharges are studied, by using an extension of the one-

*ynwang@dlut.edu.cn

 

dimensional fluid model [3]. The formation of nanoparticles is based on the larger anions ($Si_nH_{2n+1}^-$ and $Si_nH_{2n}^-$) ($n \leq 12$) in the successive chemical reactions in gas phase, and we mainly focus our attention on the transport and charging of nanoparticle with a certain radius. The presence of nanoparticles, which can greatly influence the plasma properties, such as the plasma density, ion energy, and the electric field, is also our research interest. The outline of this paper is as follows. The theoretical model is described in detail in Sec. II, whereas the simulation results of the dual-frequency effects on the dust plasma are presented in Sec. III. Conclusions are discussed in Sec. IV.

## II. THEORETICAL MODEL

### A. $SiH_4$ fluid model

A fluid model based on Refs. [3,8] is adopted to describe silane discharges in dual-frequency capacitively coupled reactor. In this model, particle density and flux balances, electron energy balance, and Poisson's equation are included, allowing self-consistent calculation of the electric field, particle densities, and fluxes.

The particle balance equation for each species $j$ (electrons, positive ions, negative ions, radicals, neutral molecules, and nanoparticles) is described by

$$\frac{dn_j}{dt} + \frac{d\Gamma_j}{dx} = S_j, \tag{1}$$

where $n_j$ is the particle's density and $S_j$ represents the creation or destruction of species $j$ by electron-impact collisions with neutrals or by chemical reactions. The flux term $\Gamma_j$ of small species (electrons, positive ions, negative ions, radicals, and neutral molecules) is estimated by drift-diffusion approximation,

$$\Gamma_j = \mu_j n_j E - D_j \frac{dn_j}{dx}, \tag{2}$$

where $\mu_j$ and $D_j$ are the mobility and diffusion coefficient. We have to notice that with much larger mass than electrons, ions cannot follow the instantaneous electric field in the discharge area. Thus, an effective electric field is introduced, and the ion flux in Eq. (2) might be changed into

$$\Gamma_i = \mu_i n_i E_{eff,i} - D_i \frac{dn_i}{dx}, \tag{3}$$

with the effective electric field $E_{eff,i}$ given by

$$\frac{dE_{eff,i}}{dt} = \frac{e}{\mu_i m_i}(E - E_{eff,i}). \tag{4}$$

Here, $e$ and $m_i$ are elementary charge and mass of the ion, respectively. The electric field $E$ and the potential $V$ are calculated from Poisson's equation,

$$\frac{d^2V}{dx^2} = -\frac{e}{\varepsilon_0}\left(\sum n_+ - \sum n_- - n_e - Z_d n_d\right), \quad E = -\frac{dV}{dx}, \tag{5}$$

where $n_+, n_-, n_e, n_d$ express the positive ion, negative ion, electron, and dust particle densities, while $\varepsilon_0$ is the permittivity of free space, and $Z_d = Q_d/e$ is the number of elementary charges on the dust particles.

TABLE I. Polarisabilities of particle and Lennard-Jones parameters.

| Particle | $\sigma$ (Å) | $\varepsilon/k_B$ (K) | $\alpha$ ($A^3$) |
|---|---|---|---|
| $SiH_4$ | 4.084 | 207.6 | 4.62 |
| $Si_2H_6$ | 4.42 | 230.0 | 8.47 |
| $H_2$ | 2.827 | 59.7 | 0.805 |
| H | 2.5 | 30.0 | |
| $SiH_3$ | 3.943 | 170.3 | |
| $SiH_2$ | 3.803 | 133.1 | |
| $Si_2H_5$ | 4.717 | 306.9 | |

The electron energy balance is introduced to calculate the electron temperature $T_e$,

$$\frac{d}{dt}\left(\frac{3}{2}n_e T_e\right) + \frac{d\Gamma_w}{dx} = -e\Gamma_e E + S_w, \tag{6}$$

where $\Gamma_w = \frac{5}{2}T_e\Gamma_e - \frac{5}{2}D_e n_e \frac{dT_e}{dx}$ is the electron energy density flux, $S_w$ is the loss of electron energy due to electron-impact collisions. No energy balances for ions, neutrals, and nanoparticles because we assume that they have local gas temperature.

In this model, to obtain the rates constant of electron-impact collisions as a function of the electron temperature, a separate module is incorporated to calculate the electron energy distribution function from the Boltzmann equation in the two term approximation, whereas the cross sections needed are given in Refs. [8,17].

For neutral particles, only the diffusion term is considered, with the diffusion coefficient $D_{ij}$ ($m^2\ s^{-1}$) of species $j$ in every background gas $i$ ($H_2, Si_2H_6, SiH_4$) obtained by the classical expression for binary collisions [17],

$$D_{ij} = \frac{3}{16}\frac{k_B T_{gas}}{P_{tot}}\frac{(2\pi k_B T_{gas}/m_{ij})^{1/2}}{\pi\sigma_{ij}^2\Omega_D(\Psi)}, \tag{7}$$

where $k_B$ is the Boltzmann constant, $T_{gas}$ is the gas temperature, $P_{tot}$ is the total gas pressure, $m_{ij}$ is the reduced mass, $\sigma_{ij} = (\sigma_i + \sigma_j)/2$ is the binary collision diameter, $\Omega_D(\Psi)$ is the diffusion collision integral with $\Psi = T_{gas}/\epsilon_{ij}$, and $\epsilon_{ij} = (\epsilon_i \times \epsilon_j)^{0.5}$. The Lennard-Jones parameters $\epsilon_j$ and $\sigma_j$ are given in Table I. The diffusion coefficient $D_j$ in the background mixed gas can be calculated by Blancs law [18] $\frac{P_{tot}}{D_j} = \Sigma_i \frac{P_i}{D_{ij}}$.

The mobility $\mu_{ij}$ of ion $j$ in background neutral $i$ (in $m^2\ s^{-1}\ V^{-1}$) is calculated by the low-field Langevin mobility expression [18],

$$\mu_{ij} = 0.514 m_{ij}^{-0.5}\alpha_i^{-0.5}\frac{T_{gas}}{P_{tot}} \tag{8}$$

where $\alpha_i$ is the polarizability of gas molecule $i$ given in Table I. Then, also by using Blancs law, we can get the ion mobility $\mu_i$ in the background mixed gas, as well as the diffusion coefficient $D_i$ based on the Einstein relationship.

### B. Nucleation process

In silane discharge, the formation of dust particles is due to a series of chemical reactions, better known as gas-phase polymerization [5,8]. Based on the numerical simulation and experiment results, we know that negative ions play an important role in the formation of dust particles. In this model, there are two different pathways to form larger silyl ($Si_nH_{2n+1}^-$) and silylene ($Si_nH_{2n}^-$) starting from $SiH_3^-$ and $SiH_2^-$,

$$SiH_3^- + SiH_4 \rightarrow Si_2H_5^- + H_2,$$

$$Si_nH_{2n+1}^- + SiH_4 \rightarrow Si_{n+1}H_{2n+3}^- + H_2, \tag{9a}$$

$$SiH_2^- + SiH_4 \rightarrow Si_2H_4^- + H_2,$$

$$Si_nH_{2n}^- + SiH_4 \rightarrow Si_{n+1}H_{2n+2}^- + H_2. \tag{9b}$$

Since vibrational excited $SiH_4$ molecules ($SiH_4^{(1-3)}$ and $SiH_4^{(2-4)}$) are proved to be important in the formation of dust particles, the molecule-anion reactions concerned with these molecules are also taken into account. A total of 36 different species (electrons, ions, neutrals, and radicals) and more than 160 reactions are included in this work. Kinds of the electron collisions and chemical reactions, as well as the reaction coefficients involved are obtained from Refs. [8,17]. Moreover, in order to avoid tracing unlimited chemical reactions in Eqs. (9a) and (9b), a step is adopted as similar work shown in Ref. [9], in which direct transforms from the large anions (mostly $Si_{12}H_{25}^-$) into nanoparticles with a given radius are introduced. That is, further anion-silane reactions, which would lead to the formation of silicon hydride anions, containing more than 13 silicon atoms (e.g., $Si_{12}H_{25}^- + SiH_4 \rightarrow Si_{13}H_{27}^- + H_2$ at $k = 10^{-18}$ $m^3$ $s^{-1}$), will be cut off and replaced by introducing the production rate as the source term to approximately describe the formation of nanoparticles with certain radii.

### C. Particle charging equation

Nanoparticles in plasmas are usually negatively charged for the thermal speed of the electrons is substantially larger than that of the positive ions. The negative charge on the nanoparticle's surface $Q_d = 4\pi\varepsilon_0 r_d V_{fl}$ is variable and mainly depends on the size of particle $r_d$ and the floating potential $V_{fl}$ relative to the surrounding plasma conditions. We can obtain the dust particle charge from the hitting of the electron and positive-ion currents toward the particle's surface [1], as

$$\frac{dQ_d}{dt} = I_i + I_e, \tag{10}$$

while neglecting the charging contribution from the anions, which cannot overcome the negative floating potential $V_{fl}$ on the dust particle. For a spherical nanoparticle with radius $r_d$, as the linearized Debye length $\lambda_L \gg r_d$, the electron current $I_e$ and ion current $I_i$ collected by the surface of dust particles can be given by the orbital motion limited theory (OML) [19],

$$I_e = -\pi r_d^2 e n_e \sqrt{\frac{8k_B T_e'}{\pi m_e}} \exp\left(\frac{eV_{fl}}{k_B T_e'}\right),$$

$$I_i = \pi r_d^2 e n_i \sqrt{\frac{8k_B T_i}{\pi m_i}} \left(1 - \frac{eV_{fl}}{k_B T_i}\right), \tag{11}$$

where $n_e$ and $n_i$ are the electron and positive-ion densities, $k_B T_e'$ is electron temperature. Also in this equation, in order to take into account, the ion drift velocity $v_i$ in the plasma sheaths, $k_B T_i$ is replaced by the mean energy $E_i$

$$E_i = \frac{1}{2} m_i v_s^2 = \frac{4k_B T_{gas}}{\pi} + \frac{1}{2} m_i v_i^2, \tag{12}$$

where $v_s = (8k_B T_{gas}/\pi m_i + v_i^2)^{1/2}$ is the mean ion speed and $v_{th,i} = \sqrt{8k_B T_{gas}/\pi m_i}$ is the ion thermal velocity as well.

### D. Particle transport equation

As for the flux term of nanoparticles, forces considered to be exerted on the particles, such as the electrostatic force, ion drag force, neutral drag force, gravitational force, as well as the thermophoretic force, are all included in this model. The electrostatic force exerted by the electric field $F_E = Q_d E$ can confine the dust particles in the discharge region. The ion drag force, formed by the collision between the positive ions and dust particles, consists of two parts [20]: one is the collection force given by $F_{i,coll} = n_i v_s m_i v_i \pi b_c^2$, representing the momentum transfer of all the ions that are collected by the dust particle; the other is the orbital force caused by Coulomb scattering of ions, expressed as $F_{i,scatt} = n_i v_s m_i v_i 4\pi b_{\pi/2}^2 \Gamma$, where $b_c$ is the collection impact parameter, $b_{\pi/2}$ is the impact parameter that corresponds to the deflection angle $\pi/2$, and $\Gamma = \frac{1}{2}\ln(\frac{\lambda_L^2 + b_{\pi/2}^2}{b_c^2 + b_{\pi/2}^2})$ is the Coulomb logarithm. The neutral drag force also results from momentum transfer between particles and neutral gas molecules, with the description [21] approximated by $F_n = -\frac{4}{3}\pi r_d^2 n_n m_n v_{th}(v_d - v_n)$, where $m_n, n_n, v_{th}$ are the background gas mass, number density, and average thermal velocity and $v_d$ is the drift velocity of dust particles, with the velocity of gas taken as $v_n = 0$. For spherical nanoparticles, the gravitational force $F_g = \frac{4}{3}\pi r_d^3 \rho_d g$ cannot be neglected in the particle's transport equation, with $\rho_d$ the mass density about $2.1 \times 10^3$ $kg/m^3$, $g$ is the gravitational acceleration. Finally, the thermophoretic force arises because of a thermal gradient of gas temperature in the plasma given by [22] $F_{th} = -\frac{32}{15}\frac{r_d^2}{v_{th}}[1 + \frac{5\pi}{32}(1-\alpha)]k_T \nabla T_{gas}$, where $k_T$ is the translation part of the thermal conductivity and $\alpha$ is the thermal accommodation coefficient of the gas, taken equal to 1. Assuming that the neutral drag force balances the sum of all other forces, the flux of nanoparticles can be expressed as a drift diffusion [23],

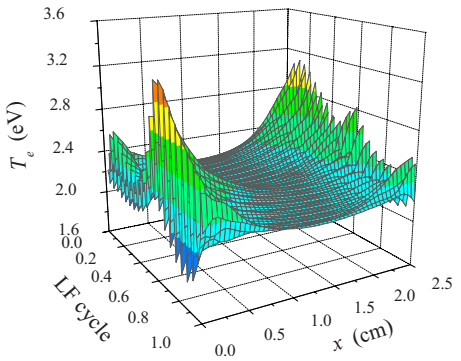


FIG. 1. (Color online) The spatiotemporal variation profiles of the electron temperature, with $P=300$ mTorr, $V_l=50$ V, $V_h=25$ V, $f_l=3$ MHz, and $f_h=60$ MHz.

$$\Gamma_d = -\mu_d n_d E_{eff} - D_d \frac{dn_d}{dx} - \frac{n_d}{\nu_{md}} g + \sum \frac{n_d m_i \upsilon_s}{m_d \nu_{md}} (4\pi b_{\pi/2}^2 \Gamma + \pi b_c^2) \Gamma_i - \frac{32}{15} \frac{n_d r_d^2}{m_d \nu_{md} \upsilon_{th}} k_T \nabla T_{gas}, \quad (13)$$

where $\mu_d = Q_d / m_d \nu_{md}$ is the nanoparticle mobility, $\nu_{md} = \sqrt{2} \frac{P_{tot}}{k_B T_{gas}} \pi r_d^2 \sqrt{\frac{8 k_B T_{gas}}{\pi m_d}}$ is the momentum loss frequency, and $D_d = \mu_d k_B T_{gas} / Q_d$ is the nanoparticle diffusion coefficient.

### E. Boundary conditions

In this work, two rf sources are applied to one electrode with the voltage $V(x=0,t)=V_h \sin(\omega_h t)+V_l \sin(\omega_l t)$ ($h,l$ represent the HF and LF sources) and the other electrode $x=L$ is set to be grounded. Moreover, boundary conditions for the differential equations specified are as follows: the electron flux at the electrodes is given by $\Gamma_e = \frac{1}{4} n_e \upsilon_{th,e} (1-\Theta)$ with the average thermal velocity $\upsilon_{th,e} = \sqrt{8 T_e / \pi m_e}$, the electron reflection coefficient $\Theta=0.25$, and the electron energy flux $\Gamma_w = \frac{5}{2} T_e \Gamma_e$, while the secondary electron emission is neglected now. The negative-ion flux at the electrodes is $\Gamma_- = \frac{1}{4} n_- \upsilon_{th,i}$, and the positive-ion flux is continuous at the electrodes $\partial \Gamma_+ / \partial x = 0$. For the neutral particles, the flux at the electrodes is given by [24] $\Gamma_n = \frac{s_i}{2(2-s_i)} n_n \upsilon_{th}$, with the sticking coefficient of neutrals $s_i = \beta_i - \gamma_i$, where $\beta_i$ is the surface reaction coefficient (representing the probability that neutrals will react at the surface) and $\gamma_i$ is the recombination coefficient (representing the probability of reaction with another adsorbed species to form a stable volatile product). The values of $s_i$, $\beta_i$, and $\gamma_i$ are given in [8].

## III. RESULTS AND DISCUSSION

In this work, we mainly study the behavior of nanoparticles and the influences of dual-frequency sources. We first set the HF source at $f_h = \omega_h / 2\pi = 60$ MHz and $V_h = 25$ V, and the LF source at $f_l = \omega_l / 2\pi = 3$ MHz, $V_l = 50$ V, with the gas pressure $P=40$ Pa (or 300 m Torr). In all calculations, the gas temperature and the electrode spacing are kept as $T_{gas}=400$ K, $L=2.5$ cm. Moreover, 100 grid points are employed in the axis direction, while one HF cycle is divided into 1000 time steps ($\Delta t \approx 1.67 \times 10^{-11}$ s). A longer time step of $1.67 \times 10^{-9}$ s is adopted for the description of the neutral-neutral chemistry to speed up the calculation. The discussion given below is based on the simulation results after calculation of 24 000 HF periods, approximately 0.4 ms. Surely, this period of time is not enough for such a system to reach perfect steady state. Actually, a cutoff is adopted in our simulations, in case of long time consuming for low convergence rate as closing to the steady state in the discharge. Anyway, we think that the simulation results present in the following are very close to the final state and few of the important physics has been lost in the following discussion.

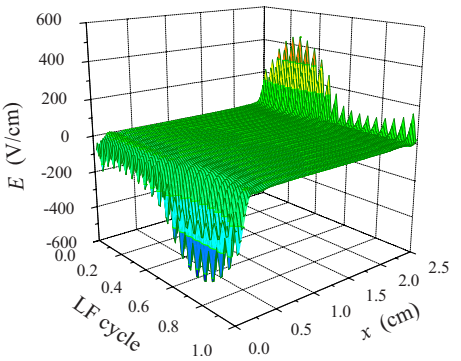


FIG. 2. (Color online) The spatiotemporal variation profiles of the electric field, with the settings the same as those in Fig. 1.

The spatiotemporal variation profiles of the electron temperature and electric field within one LF period are shown in Figs. 1 and 2, respectively. It is clear that the electron temperature shows little fluctuation in the whole space distribution but begins to oscillate obviously near the sheath region, under the influence of both the HF and LF sources. The electric field keeps nearly zero in the bulk region but becomes stronger and changes rapidly in the presheath and sheath regions, as shown in Fig. 2. Thus, the electrons accelerate significantly under the influence of the strong electric field, resulting in the evident increasing of the electron temperature in the presheath region. Figure 3 shows the spa-

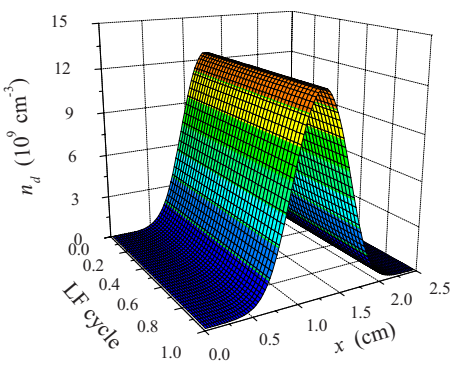


FIG. 3. (Color online) The spatiotemporal variation profiles of the nanoparticle number density, with the settings the same as those in Fig. 1.

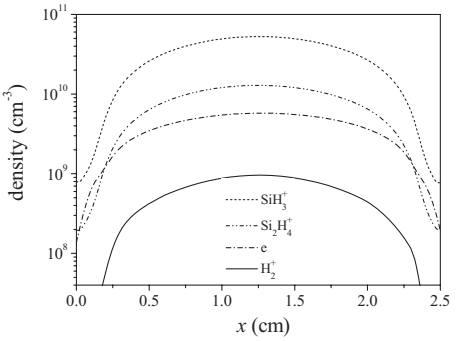


FIG. 4. The spatial variation profiles of the positive ion and electron number densities within one LF period, with the settings the same as those in Fig. 1.

tiotemporal profile of nanoparticle number density within one LF period. The figure illustrates that the nanoparticles mainly distribute in the plasma bulk. Since the electric field force exerted on the particles changes fast and far exceeds the ion drag force in the sheath regions near the electrodes, the negatively charged particles may be repelled from the plasma sheaths and effectively trapped in the bulk of the discharge.

The spatial profiles of the densities of positive ions and electron are plotted in Fig. 4, which has been time averaged in one LF period. As we can see, the most abundant positive ion in this discharge conditions is $SiH_3^+$ with a density of about $5\times10^{10}$ cm$^{-3}$ in the bulk plasma region, while the densities of the other positive ions $Si_2H_4^+$ and $H_2^+$ are approximately $1\times10^{10}$ cm$^{-3}$ and $8\times10^{8}$ cm$^{-3}$, much smaller than that of $SiH_3^+$. The electron density, as described in this figure, is about $5\times10^{9}$ cm$^{-3}$, which is almost one order of magnitude lower than that of the main positive ion $SiH_3^+$. So, after long period discharge, the presence and gradual increase in the anions along the reaction pathways in Eqs. (9a) and (9b) may take the responsibility for the decrease in the electron density. Figure 5 displays the spatial variation profiles of the densities of negative ions, including those along the two main cluster formation pathways with silyl anions ($Si_nH_{2n+1}^-$) labeled with solid lines and silylene ($Si_nH_{2n}^-$) anions with dashed lines. We can see from this figure that as the number of silicon atoms $n$ increases, the densities of the anions decrease slightly but are confined in the bulk plasma

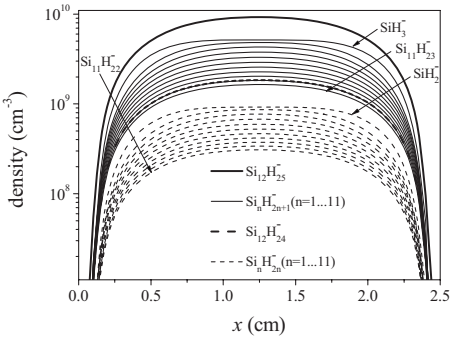


FIG. 5. The spatial variation profiles of the silyl and silylene number densities within one LF period, with the settings the same as those in Fig. 1.

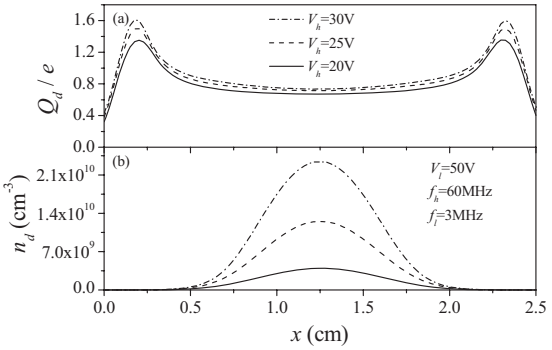


FIG. 6. (a) The average nanoparticle's charge $Q_d/e$ and (b) number density $n_d$ for different HF voltages $V_h$=20, 25, and 30 V with $V_l$=50 V, $P$=300 mTorr, $f_l$=3 MHz, and $f_h$=60 MHz.

region, showing the decreasing production of anions in the successive reaction pathway. Similar results have been also obtained in both the experimental [25] and theoretical studies [8], and the densities of all silyl anions are much higher than those of silylene anions, showing that the silyl anion reactive series is the main pathway for nanoparticles formation. We also notice from this figure that in each pathway, the densities of $Si_{12}H_{25}^-$ and $Si_{12}H_{24}^-$ are much more than the comparatively smaller anions since few loss terms leading to bigger anions is considered in this model.

Since the sheath characteristics and parameters are determined by the LF source while the plasma parameters are determined by the HF source independently, we try to fix one electric source at a certain value while adjusting the voltage or frequency of the other source to study their effects on dust particles. Here, we choose nanoparticles with radius at $r_d$ =0.5 nm. First, Figs. 6 and 7 give us effects from different voltages of HF and LF sources. Figure 6(a) shows the spatial variation profiles of the average charge $Q_d$ collected on the nanoparticle's surface, with the HF voltage $V_h$ set at 20, 25, and 30 V and the LF voltage $V_l$ at 50 V. As we know from Eqs. (10) and (11), the densities and temperatures of the ions and electron are the main parameters that the nanoparticle charge $Q_d$ depends on. The charge $Q_d$ decreases rapidly with much less electrons collision in the sheath, while exhibit prominent peaks near the presheaths for the acceleration of the electrons by rapid changes in the electric field. In the

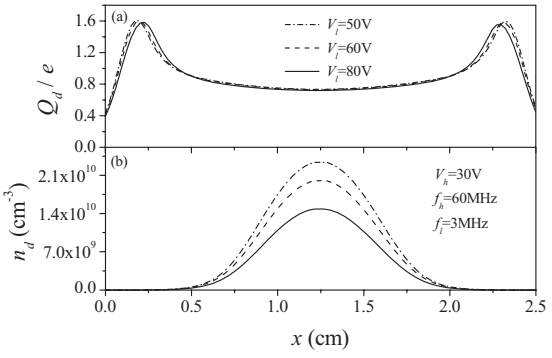


FIG. 7. (a) The average nanoparticle's charge $Q_d/e$ and (b) number density $n_d$ for different LF voltages $V_l$=50, 60, and 80 V with $V_h$=30 V, $P$=300 mTorr, $f_l$=3 MHz, and $f_h$=60 MHz.

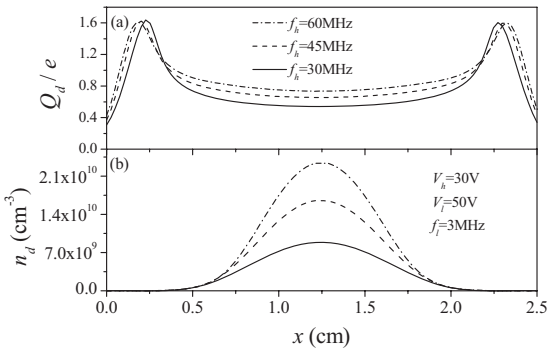


FIG. 8. (a) The average nanoparticle's charge $Q_d/e$ and (b) number density $n_d$ for different HF frequencies $f_h$=30, 45, and 60 MHz with $f_l$=3 MHz, $P$=300 mTorr, $V_l$=50 V, and $V_h$=30 V.

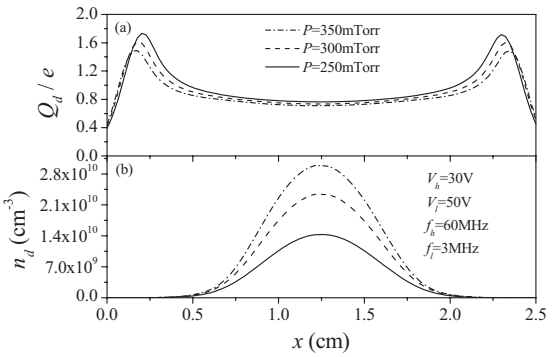


FIG. 10. (a) The average nanoparticle's charge $Q_d/e$ and (b) number density $n_d$ for different gas pressures $P$=250, 300, and 350 mTorr with $V_l$=50 V, $V_h$=30 V, $f_l$=3 MHz, and $f_h$=60 MHz.

bulk plasma, the charge on the nanoparticle gets lower because of weaker electric field and lower electron temperature. Otherwise, we can see that the nanoparticle charge increases with the increasing of HF voltage, especially in the presheath region, indicating effects on plasma parameters from the HF source. Evident effects can also be seen in Fig. 6(b), in which the spatial variation profiles of the dust particle density $n_d$ with different HF voltages are shown. It is clear that the nanoparticle densities increase definitely with the increasing of HF voltage, which is responsible for increases in the electron energy and plasma density, as well as the electric power dissipation. As for the influences of LF voltage, as shown in Fig. 7, in which the LF voltage $V_l$ has been set at 50 V, 60 V, and 80V separately, increasing of the LF voltage makes the sheath expand to the bulk plasma and the discharge power decrease, can in turn cause decreasing of dust particle density in the bulk plasma region, while slight effects are noticed on the nanoparticle surface charge.

The effects of HF and LF source frequencies on the particle are also taken into account, as shown in Figs. 8 and 9. With the HF frequency $f_h$ set at 30, 45, and 60 MHz and the LF frequency $f_l$ at 3 MHz, we can see in Fig. 8 that the nanoparticle's average charge and density increase with the increasing of HF frequency, especially in the bulk plasma region, suggesting greater electron energy and plasma densities due to higher HF frequencies and more absorption power. Moreover, compared with Fig. 6(a), the two peaks in Fig. 8(a) move nearer to the electrodes instead of just increase, indicating that more collisions between electrons and particles occur due to higher HF frequencies and result in the increase in plasma density and the shrinking of the sheaths. Thus, adjustments of HF frequency are more effective for plasma density increasing. The effects of LF source frequencies on the particle are also studied in Fig. 9, in which the plots of particle densities and charges are given in Figs. 9(a) and 9(b), with the LF frequency $f_l$ set at 3, 5, and 10 MHz and the HF frequency $f_h$ at 60 MHz. We can see that almost no special effects on the particle formation, coming from different LF frequencies. As well known, the tiny electrons in the plasma can respond to the HF frequency definitely rather than the LF frequency. Plasma is mainly produced by the collision between particles and the oscillated electrons with the HF frequency, and, according to the OML theory, the charge and density profiles of nanoparticles are dependent on the local electron and ion densities, as well as the electron temperature. Thus, the HF frequency still exerts an important influence not only on plasma discharge processes but also on nanoparticle formation. In addition, the coupling of the two applied sources will become possible when the LF frequency increases and is close to the HF frequency.

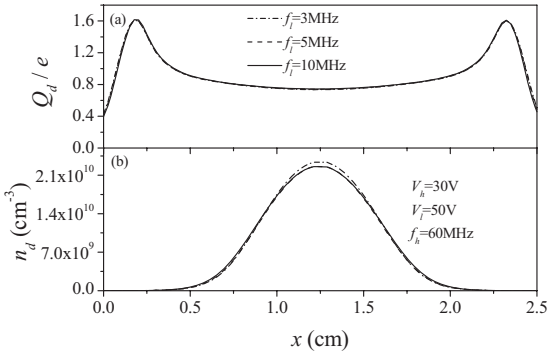


FIG. 9. (a) The average nanoparticle's charge $Q_d/e$ and (b) number density $n_d$ for different LF frequencies $f_l$=3, 5, and 10 MHz with $f_h$=60 MHz, $P$=300 mTorr, $V_l$=50 V, and $V_h$=30 V.

Figure 10 shows us the profiles of the averaged charge $Q_d$ and densities of nanoparticles, dependent on the gas pressure $P$, which has been set at 250, 300, and 350 mTorr. We can see that the nanoparticle density increases with the increasing of gas pressure, while the surface charge on the nanoparticles decreases especially in the presheath region. As the gas pressure increases, the collision between electrons and background neutrals becomes more frequent, resulting in higher plasma density and nanoparticle density, as well as larger anion density along the formation pathway of the nanoparticles. However, more larger anions' existence will lead to the decrease in the electron density due to the attachment loss in the successive polymerization reactions in the quasineutral bulk plasma. Thus, higher gas pressure can increase the nanoparticle density but shorten the averaged charge on nanoparticle surface, especially in the presheath region.

In order to figure out the effects of the existence of larger anions and nanoparticles on the plasma discharge in silane DF-CCP, we finally describe the variation in the densities of

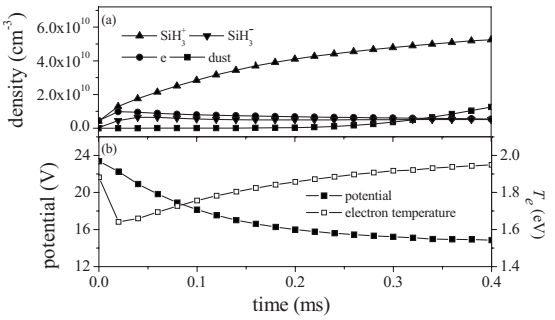


FIG. 11. The temporal variation profiles of the number densities of the particles, as well as the potential and electron temperature, in the center of the discharge, throughout the whole discharge time, approximate 0.4 ms, with $P=300$ mTorr, $V_l=50$ V, $V_h=25$ V, $f_l=3$ MHz, and $f_h=60$ MHz.

the particles, potential, and electron temperature, as a function of the discharge time, as shown in Fig. 11. The calculation results plotted in this figure are all those in the center of the discharge. Note in Fig. 11(a) that the density of the positive ion $SiH_3^+$ keeps increasing obviously from the beginning of the discharge, getting approximately one order of magnitude greater during 0.4 ms, while the dust particle with radius $r_d=0.5$ nm starts to appear from the time $t\simeq 0.2$ ms, and then its density keeps increasing definitely. Meanwhile, as the growth of larger silyl ($Si_nH_{2n+1}$) and silylene ($Si_nH_{2n}$) anions, as well as the dust particles, which always present electronegative due to different thermal speeds of the electrons and positive ions, the density of the smallest anion $SiH_3^-$ keeps decreasing after a sudden increase at the beginning of the discharge, similar to that of the electron. The electron temperature then gets increasing owing to almost the same electric power dissipation, and the electric potential decreases monotonically during the whole discharge time, as shown in Fig. 11(b).

## IV. CONCLUDING REMARKS

In summary, we have studied the influences of the dual-frequency electric sources on the formation of dust particles in silane DF-CCP by using a self-consistent fluid model, in which density and flux balances of electrons, ions, neutrals and nanoparticles, electron energy balance, and Poission's equation are included. In this simulation, 36 different species and more than 160 reactions are involved totally, and the plasma discharge lasts 24 000 HF periods, almost 0.4 ms. During this discharge, formation and transport of nanoparticles with certain radii are calculated approximately, on the basis of the largest anions $Si_{12}H_{25}^-$ and $Si_{12}H_{24}^-$.

Similar to what we have learned in capacitively coupled plasma driven by single frequency source, the HF source applied on the electrode has evident effects on the process of plasma discharge and, of course, also on the nanoparticle densities in the bulk plasma and charge distributions in the presheath region. But we also notice in this work that the relative small LF voltage in dual-frequency CCP can also accelerate the nanoparticle production, which is expected in film deposition. Moreover, the different effects of the gas pressure on the nanoparticle density and charge are discussed. Finally, the influences of the existence of dust particles and larger anions on the bulk plasma during the whole discharge time have been studied also, allowing us to know self-consistently the properties of the capacitively coupled silane discharge modulated by dual-frequency electric sources. In the future work, we will consider more about the detailed coagulation process of nanoparticles, in a two-dimensional fluid model.

## ACKNOWLEDGMENTS

This work was supported by the National Natural Science Foundation of China (Grants No. 10775025 and No. 10572035) and Program for New Century Excellent Talents in University of China (Grant No. NCET-08-0073).

[1] M. A. Lieberman and A. J. Lichtenberg, *Principles of Plasma Discharges and Materials Processing, Processing*, 2nd ed. (Wiley-Interscience, New York, 2005).
[2] Y. Watanabe, J. Phys. D **39**, R329 (2006).
[3] G. J. Nienhuis *et al.*, J. Appl. Phys. **82**, 2060 (1997).
[4] O. Leroy, G. Goussetz, L. L. Alves, J. Perrin, and J. Jolly, Plasma Sources Sci. Technol. **7**, 348 (1998).
[5] A. Gallagher, Phys. Rev. E **62**, 2690 (2000).
[6] A. Gallagher, A. A. Howling, and Ch. Hollenstein, J. Appl. Phys. **91**, 5571 (2002).
[7] W. W. Stoffels and E. Stoffels, Trends Vac. Sci. Technol. **4**, 1 (2001).
[8] K. De Bleecker, A. Bogaerts, R. Gijbels, and W. Goedheer, Phys. Rev. E **69**, 056409 (2004).
[9] K. De Bleecker, A. Bogaerts, and W. Goedheer, Phys. Rev. E **70**, 056407 (2004).
[10] K. De Bleecker, A. Bogaerts, R. Gijbels, and W. Goedheer, New J. Phys. **8**, 178 (2006).
[11] H. H. Goto, H. D. Lowe, and T. Ohmi, J. Vac. Sci. Technol. A **10**, 3048 (1992).
[12] T. Kitajima, Y. Takeo, and T. Makabe, J. Vac. Sci. Technol. A **17**, 2510 (1999).
[13] J. K. Lee, N. Y. Babaeva, H. C. Kim, O. V. Manuilenko, and J. W. Shon, IEEE Trans. Plasma Sci. **32**, 47 (2004).
[14] D. H. Kim *et al.*, J. Vac. Sci. Technol. B **23**, 2203 (2005).
[15] E. Cianci, A. Schina, A. Minotti, S. Quaresima, and V. Foglietti, Sens. Actuators, A **127**, 80 (2006).
[16] M. T. Weise, S. C. Selbrede, L. J. Arias, and D. Carl, J. Vac. Sci. Technol. A **15**, 1399 (1997).
[17] J. Perrin, O. Leroy, and M. C. Bordage, Contrib. Plasma Phys. **36**, 3 (1996).
[18] E. W. McDaniel and E. A. Mason, *The Mobility and Diffusion of Ions in Gases* (Wiley, New York, 1973).
[19] J. E. Allen, B. M. Annaratone, and U. De Angelis, J. Plasma Phys. **63**, 299 (2000).
[20] M. S. Barnes, J. H. Keller, J. C. Forster, J. A. O'Neill, and D. K. Coultas, Phys. Rev. Lett. **68**, 313 (1992).
[21] D. B. Graves, J. E. Daugherty, M. D. Kilgore, and R. K. Por-

teous, Plasma Sources Sci. Technol. **3**, 433 (1994).
[22] L. Talbot, R. K. Cheng, R. W. Schefer, and D. R. Willis, J. Fluid Mech. **101**, 737 (1980).
[23] M. R. Akdim and W. J. Goedheer, J. Appl. Phys. **94**, 104 (2003).
[24] Yu. E. Gorbachev, M. A. Zatevakhin, and I. D. Kaganovich, Zh. Tekh. Fiz. **66**, 89 (1996).
[25] A. A. Howling, L. Sansonnens, J.-L. Dorrier, and Ch. Hollenstein, J. Phys. D **26**, 1003 (1993).